Energy & Environmental Science

PERSPECTIVE

View Article Online
View Journal

Cite this: DOI: 10.1039/c5ee03887a

Colloidal quantum dot ligand engineering for high performance solar cells

Ruili Wang,†[a] Yuequn Shang,†[a] Pongsakorn Kanjanaboos,[b] Wenjia Zhou,[a] Zhijun Ning*[a] and Edward H. Sargent*[c]

Received 25th December 2015,
Accepted 8th March 2016

DOI: 10.1039/c5ee03887a

www.rsc.org/ees

Colloidal quantum dots (CQDs) are fast-improving materials for next-generation solution-processed optoelectronic devices such as solar cells, photocatalysis, light emitting diodes, and photodetectors. Nanoscale CQDs exhibit a high surface to volume ratio, and a significant fraction of atoms making up the quantum dots are thus located on the surface. CQD surface states therefore play a critical role in determining these materials' properties, influencing luminescence, defect energy levels, and doping type and density. In the past five years, halide ligands were applied to CQD solar cells, and these not only improved charge carrier mobility, but also reduced defects on the surface. With the inclusion of halide ligands, CQD solar cell certified power conversion efficiencies have increased rapidly from an initial 5% in 2010 to the latest certified values over 10%. In this perspective article, we summarize recent advances in ligand engineering that improve the performance of CQD solar cells, focusing on the use of halide inorganic ligands to improve CQD surface passivation and film conductivity simultaneously.

Broader context

Sustained growth in energy demand has stimulated continued research in next-generation solar photovoltaic technologies. Among new technology pathways, colloidal quantum dots (CQDs) have received considerable recent attention in light of their manufacture *via* solution processing methods, and also their bandgap tunability that enables full visible + infrared spectral havesting. CQD solar cells have advanced rapidly in solar power conversion efficiency from 5% to greater than 10% in the past five years. The present perspective summarizes the physical and chemical origins of CQD photovoltaic improvements, focusing particularly on how the nanoparticles' surfaces are managed *via* ligand engineering. The translation of these chemical strategies into improved physical electronic properties such as carrier mobility and reduced defect density is explored, and ever-improving device models reveal how these have enabled advances in performance and set the stage for continued progress.

Introduction

Colloidal quantum dots (CQDs) combine bandgap tunability with the attraction of solution-based fabrication. Their excellent optical absorption characteristics,[1–4] especially in the infrared region, coupled with the prospect of multi-exciton generation (MEG),[5–7] make CQDs of interest in the realization of both solar cells[8–11] and photodetectors.[12,13] Their high photoluminescence quantum yields (PLQY) and sharp emission peaks enable CQD-based light emitting diodes (QDLEDs) for next-generation display technologies.[14–16]

The performance of CQD optoelectronic devices has improved dramatically in recent years. The certified efficiency of CQD solar cells reached 10.6% early in 2016,[17] consistent progress considering that the efficiency was below 0.1% one decade ago. The use of PbTe CQDs exhibiting MEG led to reports of external quantum efficiencies of approximately 120%.[18] High definition displays have been commercialized that rely on CQDs to achieve excellent color purity.[19] The external quantum efficiency (EQE) of CQD-based light emitting diodes (LED) recently exceeded 20%.[20–23] Field effect transistors (FETs) based on CQD inks have shown charge carrier mobilities comparable to those of the best solution-processed semiconductors.[24] Infrared photodetectors that rely on CQDs for light absorption and photocharge generation are reaching the mobile camera market at 2016.[25] In recent years, CQDs have been explored for solar cell light concentrators,[8,26–32] thermoelectric devices,[33–37] and lasers.[38–40]

[a] School of Physical Science and Technology, ShanghaiTech University, Haike Road 100, 201210 Shanghai, China. E-mail: ningzhj@shanghaitech.edu.cn
[b] Materials Science and Engineering, Faculty of Science, Mahidol University, 272 Rama 6 Road, Ratchathewi District, Bangkok, Thailand 10400
[c] Department of Electrical and Computer Engineering, University of Toronto, 10 King's College Rd, Toronto, Ontario M5S 3G4, Canada. E-mail: ted.sargent@utoronto.ca
† These authors contributed equally to the work.

Key breakthroughs were made in the synthesis of monodispersed CQDs nearly 3 decades ago.[41–46] Early device prototypes showed low performance that originated from low carrier mobilities resulting from the inclusion of long insulating alkyl chain ligands in the quantum dot solid. A new paradigm of the conduction-compatible ligand emerged in the past decade, wherein researchers explored short ligands as passivants such as the metal chalcogenide complexes (MCCs). These resulted in much improved carrier mobility and film conductivity.

However, bipolar optoelectronic devices such as solar cells and LEDs rely on excited state lifetimes that ideally come close to the radiative lifetime in the quantum dot. A high density of recombination centres produced rapid nonradiative recombination, hence low radiative efficiency and short excited state lifetimes. This was associated with the surface of the quantum dots, whose area is large relative to the volume of semiconductor bulk, especially when compared to the case of microcrystalline materials.

The consequent focus of the research community has therefore been on the CQD surface, and this has been the foundation of many of the past five years' improvements in CQD materials electronic properties and device performance. In one key example, the application of halide ligands has reduced surface defects and led directly to much improved power conversion efficiencies in solar cells (PCE).[47] In a parallel vein, the introduction of a passivating perovskite matrix has offered a new strategy to manage the CQD surface and also added into the CQD toolkit new functional elements, such as matrix-based light absorption, excited state transport, and injection of photocharges.[48]

In this Perspective, we summarize the latest advances in CQD surface engineering, with our focus on those that have

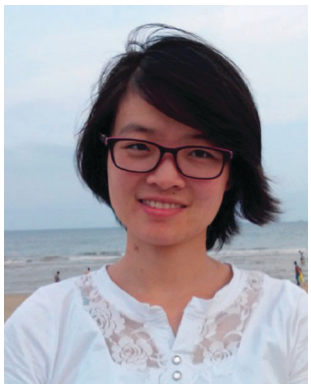

Ruili Wang

Ruili Wang is a PhD student in the School of Physical Science and Technology at ShanghaiTech University. She received her Bachelor's degree in materials science and engineering from Zhengzhou University in 2013. Currently, she is conducting her PhD studies under the supervision of Prof. Zhijun Ning. She is exploring new materials and surface engineering to enhance the performance of quantum dot solar cells.

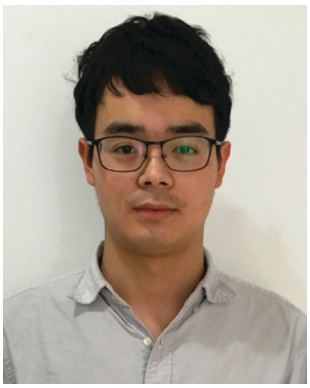

Yuequn Shang

Yuequn Shang is currently a PhD candidate under the guidance of Prof. Ning in the School of Physical Science and Technology at ShanghaiTech University. He received his BS in the School of Physics and Optoelectronic Engineering from Xidian University, China in 2014. His current research focus is on perovskite and nanomaterial based optoelectronics.

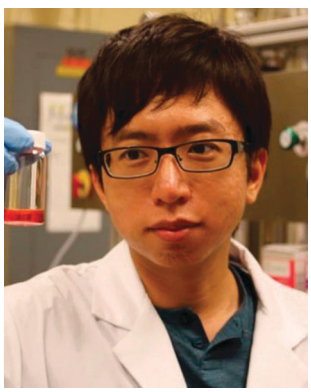

Pongsakorn Kanjanaboos

Pongsakorn Kanjanaboos received his B.A. in physics and economics from Washington University in Saint Louis in 2008. He earned his Ph.D. in physics from the University of Chicago in 2013. In collaboration with Argonne National Laboratory, he investigated self-assembly, nanomechanics, and application of solution-processed nanoparticle thin films. Because of his interests in both academic and business sides of R&D, he also studied business at the University of Chicago Booth School of Business. In 2013, Pongsakorn joined the Department of Electrical and Computer Engineering at the University of Toronto as a postdoctoral fellow to work on solution-processed semiconductors. Currently, Pongsakorn holds a faculty position at Materials Science and Engineering, Faculty of Science at Mahidol University in Thailand. His current research interests include nanomechanics, coating technologies, and solution-processed semiconductors such as colloidal quantum dots and perovskites.

Wenjia Zhou

Wenjia Zhou received his Bachelor's degree in material chemistry from Sichuan University in China in 2009. He earned his PhD in physics from the Institute of physics, the Chinese Academy of Sciences in 2015, where he worked on fabricating perovskite oxide films and studying their photoelectricity properties. In 2015, Wenjia Zhou joined the School of Physical Science and Technology at ShanghaiTech University as a postdoctoral fellow to work on solar cells, photodetectors, and other optoelectronic devices from solution-processed semiconductors such as colloidal quantum dots and perovskites.

demonstrably contributed to increased optoelectronic device performance. We zoom in on the critical and multiple roles of surface ligands, and explore how the chemistry of ligand exchanges impacts surface chemistry and, ultimately, performance. We begin (Section 1) with a presentation of organic ligands used in CQD synthesis. Inorganic MCC ligands (Section 2), successfully developed to increase carrier mobility, are then discussed. Halide ligands (Section 3) that achieve low defect density while retaining high carrier mobility are followed; and their use to reduce defects in mixed organic–inorganic materials (Section 4) is shown. Lastly, we discuss a new family of materials, CQDs in a perovskite matrix (Section 5).

1. CQDs with organic ligands

1.1 Solid-state ligand exchange. The synthesis of CQDs depends on the use of long alkyl chains such as oleic acid or oleylamine.[49–56] These insulating molecules block interdot carrier transport. Hence, for optoelectronic devices, it was necessary to replace the original long alkyl chains with short ligands, such as mercaptopropionic acid (MPA) and 1,2-ethanedithiol (EDT).[57–63] Two primary methods exist for ligand exchange: solid-state and solution-phase.

The scheme for solid-state ligand exchange is shown in Fig. 1a. CQDs with long alkyl ligands are deposited onto the substrate by spin-coating, after which a solution containing short organic ligands such as MPA or EDT[28,59,60,64,65] is deposited on the film. Following a short soaking time and the removal of the solution by spin-coating, a protic solvent is cast onto the film to wash away the exchanged ligands as well as the excess of new short ligands. To ensure complete ligand exchange, the CQD concentration is carefully adjusted to allow the thickness of each layer to be typically in the few 10 s of nm. For solar cells, roughly 10 layers are needed to obtain the thickness that is optimal today in light harvesting.

The second approach involves solution-phase ligand exchange (Fig. 1b), in which one mixes together CQDs capped with long alkyl chains dispersed in a nonpolar solvent with short hydrophilic organic ligands dissolved in a polar solvent. CQDs become encapsulated with the short hydrophilic ligands and transfer into the polar solvent. The exchanged CQDs in the solution can then function as an ink, facilitating a one-step film fabrication procedure wherein spin-coating or spray-coating is carried out without the need for further exchange steps.

At present, most high-performing CQD solar cells rely on solid-state ligand exchange: it is a widely mastered method that produces smooth and compact CQD films whose long alkyl ligands are substantially removed. The strong binding between thiol ligands and CQDs enables fast and efficient exchange. IR spectra and thermal gravimetric analysis[27] show that the original organic ligands are efficiently removed. The well-defined excitonic absorption peak seen in a dispersion of same-sized CQDs is maintained in the CQD solid, indicating the quantum confinement properties left substantially intact.

Transport in these CQD solids is limited: CQD films with short organic ligands typically show mobilities that reside below 10^{-2} cm^2 V^{-1} s^{-1}. Conjugated organic ligands such as *N*-2,4,6-trimethylphenyl-*N*-methyldithiocarbamate were explored; however, no major carrier mobility improvement was observed, possibly due to poor carrier transport between the CQDs and the organic ligands.[66] Various solar cell structures, such as Schottky,[67] heterojunction,[68] and bulk heterojunction[69] have been developed for CQD solar cells with small organic ligands,[69] and their solar PCEs are generally limited to about 6%.[67,70,71]

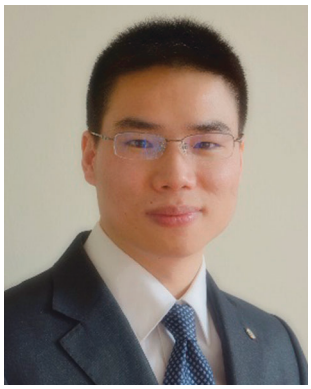

Zhijun Ning

Zhijun Ning received his PhD degree from Department of Applied Chemistry, East China University of Science and Technology. From 2009 to 2011, he was a Postdoctoral Scholar at Royal Institute of Technology, Sweden. From 2011 to 2014, he was a Postdoctoral Scholar in the Department of Electrical and Computer Engineering, University of Toronto. Since December 2014, he holds a faculty position at School of Physical Science and Technology, ShanghaiTech University. He received the Chinese Young 1000 program award in 2015. His publications have been cited over 3000 times. His current research interest focus on solution processed optoelectronic materials, especially leveraging chemistry method to address interface and surface management in nanomaterials.

Edward H. Sargent

Ted Sargent received the B.Sc.Eng. (Engineering Physics) from Queen's University in 1995 and the PhD in Electrical and Computer Engineering (Photonics) from the University of Toronto in 1998. He holds the rank of University Professor in the Edward S. Rogers Sr. Department of Electrical and Computer Engineering at the University of Toronto. He holds the Canada Research Chair in Nanotechnology and also serves as Vice-Dean for Research for the Faculty of Applied Science and Engineering. He is founder and CTO of InVisage Technologies and a co-founder of Xagenic. He is a Fellow of the Royal Society of Canada; a Fellow of the AAAS "... for distinguished contributions to the development of solar cells and light sensors based on solution-processed semiconductors;" and a Fellow of the IEEE "... for contributions to colloidal quantum dot optoelectronic devices." His publications have been cited over 15 000 times.

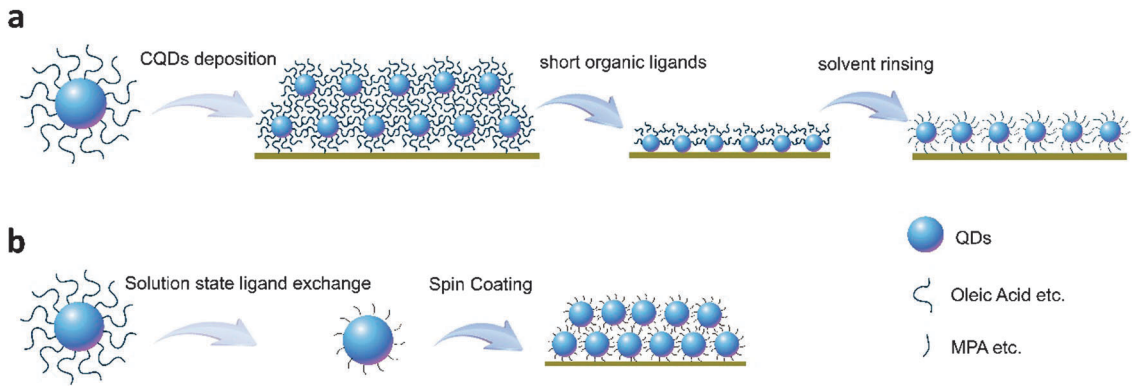

Fig. 1 (a) Schematic diagram of solid state ligand exchange and film fabrication. CQDs were firstly deposited on substrate by spin coating, then short organic ligands in solvent were dropped on CQD film to replace the long alkyl chains. After that, protic solvent was used to rinse the exchanged ligands. (b) Schematic diagram of solution phase ligand exchange and film fabrication. Firstly, long alkyl chain ligands were exchanged into short organic thiol ligands in solution. One step spin coating process was then used for film fabrication.

1.2 Solution-phase ligand exchange. Electronic defects associated with underpassivated CQD surfaces result in low operating voltages as well as low carrier mobilities. Ligand loss can occur during solid-state ligand exchange, especially when a protic solvent is employed (Fig. 2).[72] Solution-phase ligand exchange in a non-protic solvent was therefore developed: inks based on MPA-ligated CQDs have, for example, been developed, and showed initially promising PCEs when applied in a single-step drop-casting process.[73] Arenethiolate ligands[71] have also been employed in solution-phase exchange efforts, though to date with low device efficiencies. In comparison with traditional semiconductors prepared *via* dry methods, solution-phase processes introduce an added degree of freedom: solvents can have multiple effects. Firstly, the binding between solvent molecules and CQD surface atoms and ligands need to be considered. In addition, the concentration of ligands and CQDs play an important role in the dielectric constant of the solution, which can in turn impact the properties of CQDs. For these reasons, the solution state ligand exchange depends on the type of solvent, the CQDs, the ligands, and each needs precise control. Once each of these factors is rendered consistent, the reproducibility of ligand exchange and the resultant device performance are expected to compare well with traditional dry semiconductor processes.

To improve device performance, a centrifugal casting process was developed for the fabrication of films based on CQD inks (Fig. 3a).[74] CQDs of different sizes were deposited in a one-step process, providing a convenient means to fabricate a graded solar cell structure to improve carrier collection. Solar performance was increased in this fashion by more than twofold over relevant controls. Photodetectors based on this new fabrication strategy showed impressive normalized detectivities of 2.4×10^{13} Jones (I Jones = 1 cm $Hz^{1/2}$ W^{-1}).

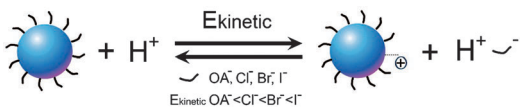

Fig. 2 Ligand loss as the interaction between proton and CQD surface ligands. The kinetic energy ($E_{kinetic}$) of ligand desorption on CQD surface is increased from oleic acid, chloride, bromide to iodide.

Solution-phase organic ligand exchanges have also been employed in the realization of CQD sensitized solar cells.[75–77] Short thiol ligands based on the carboxy unit replaced long original alkyl ligands to enable dispersion of CQDs in an aqueous solvent. The end carboxy unit anchors CQDs to the TiO_2 surface. In contrast with thin film solar cells, a liquid electrolyte is included in CQD sensitized solar cells: a sulfide compound is the most frequently used redox couple in the electrolyte. In light of the strong binding capability of sulfide ions to the CQD surface, it has the potential to replace the original ligands, thereby weakening the effect of ligands on the performance of solar cells. The passivation of a number of organic ligands to CdS and CdS/ZnS CQDs has been explored in QD-sensitized solar cells.[78] Amine and thiol groups bring higher efficiencies compared with the acid group. When a solid state electrolyte was used, the effect of the ligand became more obvious still. The addition of the tripeptide L-glutathione doubled the device performance.[79]

While a tradeoff generally exists between defects and transport when organic ligands (even short ones) provide the sole basis of surface passivation, the compromise is a more acceptable one in electroluminescence. Here, thiol ligands have been generally used in CQD based LEDs that passivate CQDs well and bring high film PLQYs.[80–82] For infrared CQDs, long thiol ligands have enabled luminescence external quantum efficiencies (EQE) exceeding 2%.[83] Recently, in the visible region, Peng *et al.* achieved EQEs above 20% based on CdSe/CdS CQDs capped with thiol ligands.[20]

2. Molecular metal chalcogenide complexes (MCCs)

To increase carrier mobility, inorganic MCC ligands were developed:[84] in contrast with organic alkyl chains, MCC ligands usually provide a net charge, allowing dispersion in highly polar solvents. A typical reaction for the synthesis of $[In_2Se_4]^{2-}$ MCC ligands may be written:[85]

$$5N_2H_4 + 2Se + 2In_2Se_3 \rightarrow N_2 + 4N_2H_5^+ + 2[In_2Se_4]^{2-}. \quad (1)$$

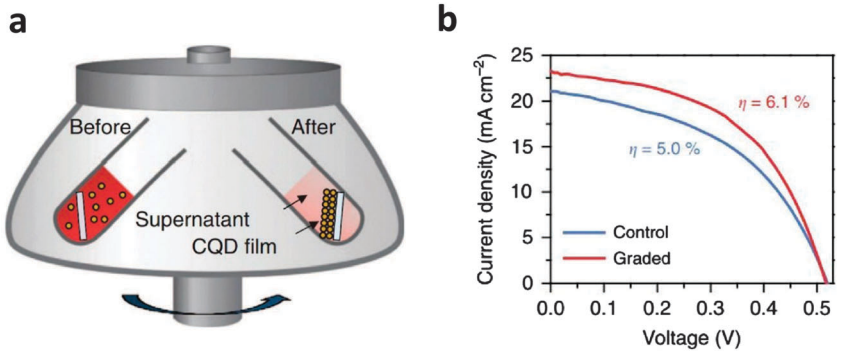

Fig. 3 (a) Schematic diagram showing CQD film fabrication by centrifugal casting. (b) Current–voltage (J–V) characteristic for devices employing ungraded (blue) and graded (red) CQD devices under AM 1.5 simulated solar illumination. The device performance with graded structure is higher than that with ungraded one.

Chalcogenide anions bind strongly with cations on CQD surfaces, replacing the original organic ligands. As shown in Fig. 4, before ligand exchange, CQDs are dispersed in hexane, the top phase. After ligand exchange, CQDs are transferred into the bottom hydrazine phase.[84] Fourier transform infrared (FTIR) spectra (Fig. 5a) demonstrate almost no signal from organic components, a finding reinforced by thermogravimetric analysis (TGA). Using a high-polarity solvent with a dielectric constant similar to that of the CQDs produces well-dispersed materials whose absorption peaks remain intact following ligand exchange (Fig. 5b). Transmission electron microscopy (TEM) images of CQDs (Fig. 5c and d) reveal no obvious change in shape and monodispersity following the ligand exchange. MCC ligands have now been successfully developed for CQDs ranging from CdSe, $CuInS_2$, InAs, $Cu_{2-x}Se$, CdS, to PbS.[24,86–90] In addition to metal inorganic complexes, pure anion ligands such as S^{2-}, HS^-, Se^{2-}, HSe^-, Te^{2-}, HTe^-, TeS_3^{2-}, OH^-,[91] and NH^{2-}, PO_4^{3-} have also been deployed.[92]

Similar to the case of CQD inks based on organic ligands, one-step spin coating can be explored for film formation directly from MCC-ligated CQDs. Organic components such as ammonium can be removed *via* a mild post-anneal.[85] Following the removal of organic ligands, both carrier mobility and conductivity are considerably enhanced, allowing impressive CQD-based field effect transistors to be demonstrated. Compared with traditional FETs based on bulk crystalline materials, direct solution fabrication simplifies and reduces the cost of device fabrication. The application of MCC-capped InP and InAs CQDs for FETs[87] has led to remarkable electron mobilities of 16 $cm^2\ V^{-1}\ s^{-1}$ in the linear regime and 14.8 $cm^2\ V^{-1}\ s^{-1}$ in the saturation regime.

A high carrier mobility has also enabled solution-processed photodetectors (Fig. 6a). By using $In_2Se_4^{2-}$ MCC ligands for CdSe/CdS core–shell CQDs, holes were confined in view of the shallower valence band of the ligands, while electrons were able to move smoothly through ligands (Fig. 6b), as a result, a remarkable gain value was obtained. The combination of high carrier mobility and gain value give rise to an impressive detectivity ($D^* > 1 \times 10^{13}$ Jones (Fig. 6c)).[93]

Recently, by using $[CdTe]^{2-}$ MCC ligands, CdTe CQD films show carrier mobility of 200 $cm^2\ V^{-1}\ s^{-1}$ (Fig. 6d and e), a value comparable to those of the best bulk solution-processed materials.[94] Since the composition of MCC ligands was the same as that of the CQDs, MCC ligands acted as molecular solders to connect otherwise-separate nanocrystals,[94] accounting for the electrical continuity and thus high mobility of the inorganic solid.

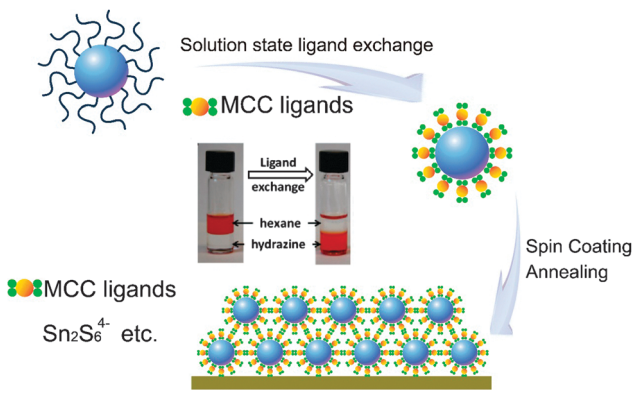

Fig. 4 Schematic diagram of MCC ligand exchange and film fabrication process. Firstly, organic ligands were exchanged into MCC ligands in solution. After that, spin coating was used to fabricate the film. (Inset: The images of MCC ligand exchange.)

3. Halide ligands

3.1 Halide ligand passivation. Although the charge carrier mobility of CQD films has been improved impressively by the use of MCC ligands, solar cell performance based on MCC ligands has yet to be reported, a finding ascribed to these solids' high density of defects.[95] To reduce defect density while keep high carrier mobility, halide ligands have been explored for CQD passivation. The atomic sizes of halide ligands allow efficient carrier transport between CQDs; while the strong binding of halides to CQD surfaces offers the capacity to improve surface passivation.

Precursors based on halide salts had previously been used in CQD syntheses; however, little attention was paid at that time to the halides' surface passivation benefits. In early work applying halide ligands to CQDs in the solid state,[95] organic ligands were replaced using halide ligands, while the absorption

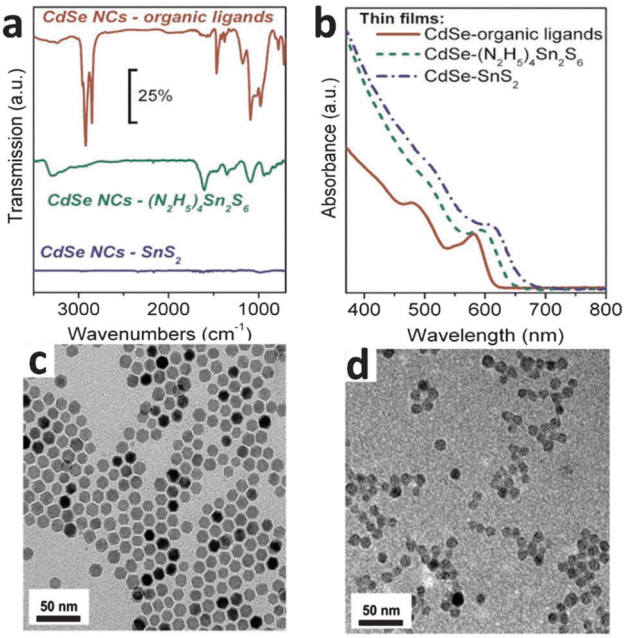

Fig. 5 (a) FTIR spectra for 3.6 nm CdSe CQDs capped with long-chain organic ligands (red line) and with $(N_2H_5)_4Sn_2S_6$ ligands before (blue line) and after (green line) annealing. Organic component was effectively removed after annealing process. (b) Absorption spectra collected using an integrating sphere for thin films composed of 4.6 nm CdSe CQDs capped with original organic ligands (red line) and with $(N_2H_5)_4Sn_2S_6$ ligands before (blue line) and after (green line) annealing. The shape of the absorption spectra was kept after annealing process. (b and c) Was reprinted with permission from ref. 90. Copyright 2012 American Chemical Society. (a and d) Was reprinted with permission from ref. 84. Copyright 2009 American Association for the Advancement of Science. TEM image of as synthesized, oleylamine capped (c) and $[In_2Se_4]^{2-}$ MCCs capped (d) $Cu_{2-x}Se$ CQDs. No obvious change of the CQD shape was observed before (c) and after (d) the ligand exchange.

excitonic spectral feature was retained. In comparison with the case of organic ligands, the defect density was reduced while the charge carrier mobility was appreciably improved to over 10^{-2} cm^2 V^{-1} s^{-1}. This first example of actively engineering CQD surfaces using halide ligands led to the first certified solar cell power conversion efficiencies that exceeded 5% in CQD solar cells.

Since the use of a protic solvent in solid-state ligand exchange can cause the loss of ligands,[61] it was crucial to develop new ligands that can bind more strongly to CQD surfaces, resisting these solvents. In comparison to bromide and chloride ligands, iodides were found to form stronger bonds to the CQD surface atoms[72] (Fig. 7a). The use of iodide ligands brought much lower film defect density. These experimental results were explained *via* soft/hard base/acid theory: the soft base iodide bound strongly to soft acid lead atoms on PbS CQDs,[96] while hard acid hydrogen cations bound strongly to hard base chloride. In comparison to iodide, chloride on PbS CQD surfaces is easily removed by a protic solvent. Density function theory (DFT) simulations confirmed that the energy needed to remove iodide ligands is indeed expected to be much greater than that of chloride.[72]

Recently, based on DFT simulation, the binding of oxygen was found to give rise to defects in the bandgap, while the adsorption of halide ligands prevents oxygen adsorption. (Fig. 7b and c)[97,98] The device operates stably in air under AM1.5 illumination for more than 100 hours. This was consistent with experimental results that confirm a lower level of oxygen on CQD surfaces when halide ligands are used.[61]

3.2 Physical property engineering. The improved understanding of CQD surface composition and its significance enabled advanced surface engineering techniques to be deployed toward the goal of controlling films' physical properties (Fig. 8a). Based on computational studies, films' doping types and doping densities are tied to surface composition: guidelines were introduced, such as the observation that ligands with negative-one charge brings an n-type film, while negative-two charge ligands such as oxygen cause p-type films. The reduction of halide ligands can cause CQD oxidation and a decrease in n-type doping density.[99]

The use of iodide brings a higher n-type doping density (Fig. 8b) in light of its high density on the surface of CQDs. This allowed gradient doping, such as the use of iodide ligands for a highly-doped layer and bromides for a lightly doped n-type film (Fig. 8c).[100] Compared to a single CQD layer exhibiting a high doping density, the graded device structure had a more extended depletion region, and at the same time the operating voltage was increased. These factors combined led to an overall increase of 1.2× in device performance. Based on a similar device structure, n-type CQD solids were combined with top EDT-ligated p-type CQD films for a notable 2014 advance in certified solar PCE (Fig. 9a).[101] Device performance was maintained for more than 150 days when the device was stored in air.

Considering the high surface to volume ratio, the change of surface ligands may reasonably be expected also to bring dramatic shifts in energy levels relative to vacuum. Electron donating thiol ligands lift up energy levels, while electron-accepting ligands such as halides downshift energy levels (Fig. 9b).[101,102] The analogy has been drawn to the case of organic chromophores, in which the energy levels are adjusted *via* the choice of substituents.

3.3 Solution phase iodide ligand exchange. To further increase ligand passivation in final CQD solids, solution-phase halide ligand exchanges were recently developed (Fig. 10). Tetrabutylammonium iodide salts were dissolved in oleylamine and the solution was then mixed with CQDs in toluene. PLQY values were increased typically 1.3× a result of the ligand exchange.[103] Compared with solid-state ligand exchange, the lack of steric hindrance in the solution phase treatment increased accessibility and binding. The defect density of films was ultimately reduced one order of magnitude and the carrier mobility of films improved to over 10^{-1} cm^2 V^{-1} s^{-1}. Recently, the combination of solution-phase molecular iodine treatment and gradient doping structure led to certified efficiencies of 9.9% (Fig. 11a and b).[104] For 49 devices, the deviation of the device efficiency is ±0.2%, indicating high reproducibility.

In-solution iodide passivation prevents the formation of defects induced by the protic solvent washing process.[61] The combination of the solution phase iodide treatment and the

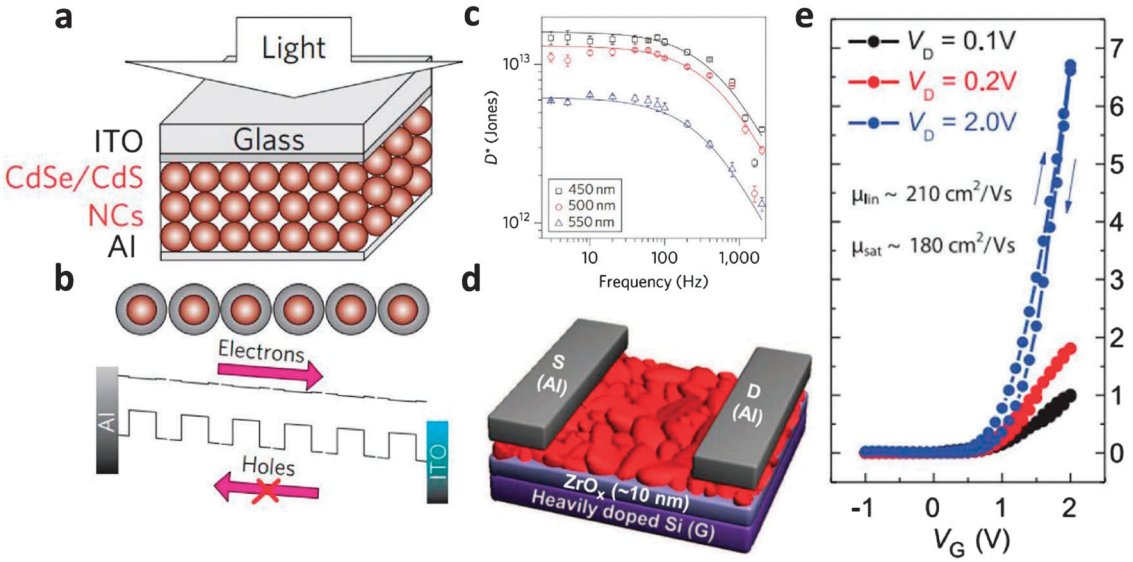

Fig. 6 (a) Scheme of a photoconductor based on CdSe/CdS core/shell CQDs with $[In_2Se_4]^{2-}$ MCC ligands. (b) Energy level structure of the CQD film. The holes are confined in CdSe core, while electrons can move smoothly in the film. (c) The detectivity of the photoconductor with different illumination wavelength. The highest detectivity is over 10^{13} jones. (d) FET device with 10 nm ZrO_2 gate dielectric and Al source and drain electrodes. (e) Transfer characteristics and of an FET with a channel made of spin-coated $[Cd_2Se_3]^{2-}$ capped CdSe CQDs. The highest carrier mobility is over 200 $cm^2 V^{-1} s^{-1}$. (a)–(c) was reprinted with permission from ref. 93. Copyright 2011 Nature Publishing Group. (d and e) Was reprinted with permission from ref. 94. Copyright 2015 American Association for the Advancement of Science.

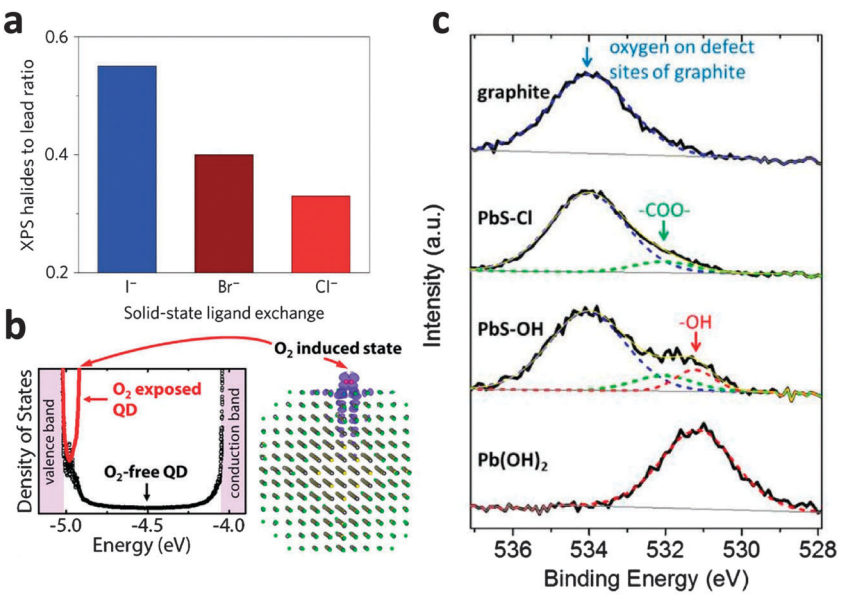

Fig. 7 (a) Halide ligand to lead atomic ratio of CQD films after the solid-state halide ligand exchange. The amount of iodide ligands is much higher than chloride and bromide. (b) Molecular oxygen induces in-Gap states for PbS quantum dots. (c) The XPS (X-ray photoelectron spectroscopy) spectra of PbS CQDs with or without the use of chloride ligand. A new peak from Pb–OH group is observed for CQDs without chloride ligand, indicating that the use of halide can effectively prevent surface oxidation and the formation of defects. (a) Was reprinted with permission from ref. 72. Copyright 2014 Nature Publishing Group. (b) Was reprinted with permission from ref. 97. Copyright 2015 American Chemical Society. (c) Was reprinted with permission from ref. 98. Copyright 2014 American Association for the Advancement of Science.

solid state iodide ligand exchange increased iodide ligand amounts on CQD surfaces, allowing better surface passivation while reducing surface oxidation. The increase in the iodide level gives rise to a more heavily n-type doped film.[105] As a result, by combining both the solution state and the solid state iodide ligand exchange, air stable n-type CQD films were prepared for the first time.[95] The CQD film, prepared in a glovebox, remained stably n-type in air, and could thus be later overcoated with p-type CQD film processed air, enabling the first inverted quantum junction solar cells.[71] For 24 devices,

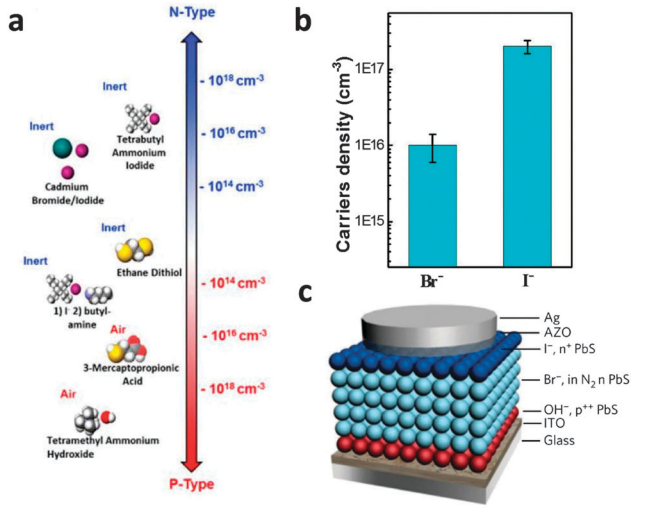

Fig. 8 (a) Illustration of the doping type and density of various ligands for PbS CQDs. The use of halide ligands brings n-type doping, while the use of organic ligands in air gives rise to p-type doping. (b) Carriers density of the films with the use of bromide and iodide ligands respectively. The film with iodide as the ligand show higher carriers density than bromide. (c) Graded doping structure device with the combination of p^+ type, n-type and n^+ type CQD films. This structure effectively extends the depletion region of the device. (a) Was reprinted with permission from ref. 99. Copyright 2012 American Chemical Society. (b and c) Was reprinted with permission from ref. 100. Copyright 2013 John Wiley and Sons.

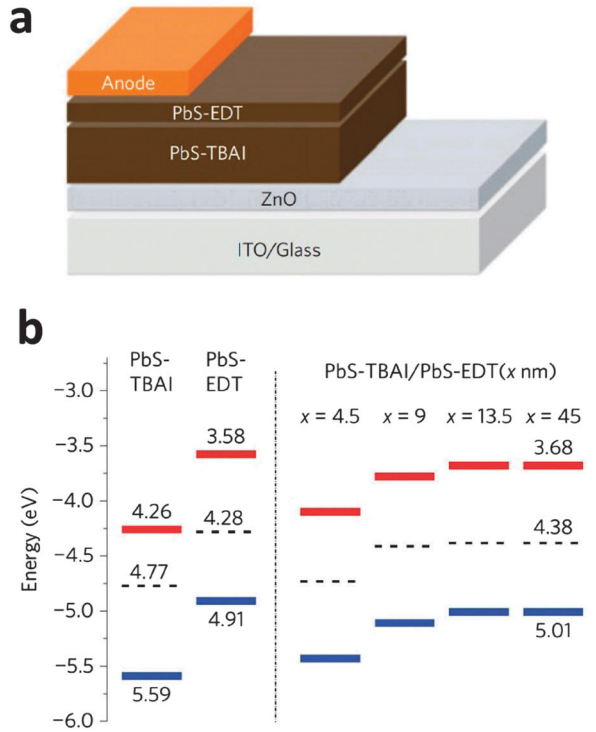

Fig. 9 (a) Device architecture of CQD solar cells with ZnO as n-type layer, CQDs with iodide ligands as inter layer, and CQDs with EDT as the top p-type layer. (b) Energy levels with respect to vacuum for pure PbS-TBAI, pure PbS-EDT and PbS-TBAI films covered with different thicknesses of PbS-EDT layers (TBAI is the abbreviation of tetrabutylammonium iodide). Reprinted with permission from ref. 101. Copyright 2014 Nature Publishing Group.

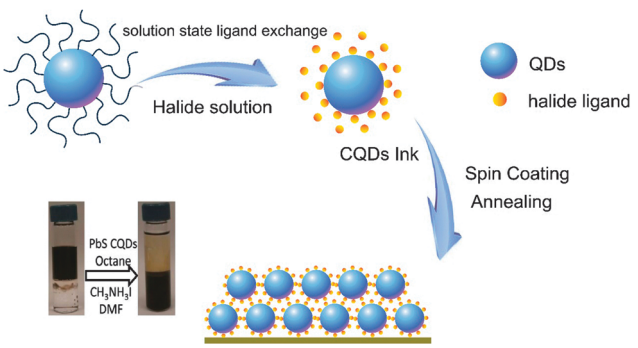

Fig. 10 Schematic diagram of solution phase halide ligand exchange. Firstly, halide was used to replace all organic ligands in solution. One step spin coating was used for film fabrication, followed by an annealing process. The image inside shows the ligand exchange process.

the deviation of the device efficiency was ±0.4%, indicating good reproducibility. In this device, the depletion region was increased as both p-type and n-type films had only moderate final/net doping densities, allowing an increase in the thickness of the active layer. Improved light harvesting capability in the infrared spectral region was achieved in this fashion.[72]

Although the solution-phase halide ligand treatment partly replaces organic ligands, the exchange was not complete and the solid-state ligand exchange process was still needed to remove organic ligands completely. Using CH_3NH_3I as the iodide source for the solution-phase ligand exchange of CdSe CQDs was found to allow complete replacement of the original organic ligands with halide ligands.[106] The exchanged CQDs were applied to create CQD sensitized solar cells formed *via* electrophoretic deposition. An analogous solution-phase halide ligand exchange process (Fig. 10) was developed for PbS CQDs.[107] CQDs were transferred from the top octane phase to the bottom *N*,*N*-dimethylformamide (DMF) phase following ligand exchange. The absorption and emission spectra were kept well after ligand exchange. A combination of CH_3NH_3I and PbI_2 was also employed, leading to well-retained luminescence quantum yields post-exchange.[107]

For CQDs with inorganic ligands such as MCCs or halides, high polarity solvents are used to disperse the exchanged CQDs. Due to the weak bonding between ligands and solvent molecules, halide ligands are lost after the solvent evaporates. To solve this problem, butylamine, with its low polarity and weaker interaction with CQD surface ligands, was employed. Absorption and emission peaks were preserved in film, and the efficiency of CQD ink-based solar cells increased to a record (at that time, 2014) of 6% PCE.

4 Hybrid ligands

Hybrid materials that combine organic crosslinkers and inorganic passivants have drawn significant attention in recent years.[77,108–110] The hybrid ligand passivation scheme (Fig. 12) contains two steps: solution-phase halide ligand exchange followed by a

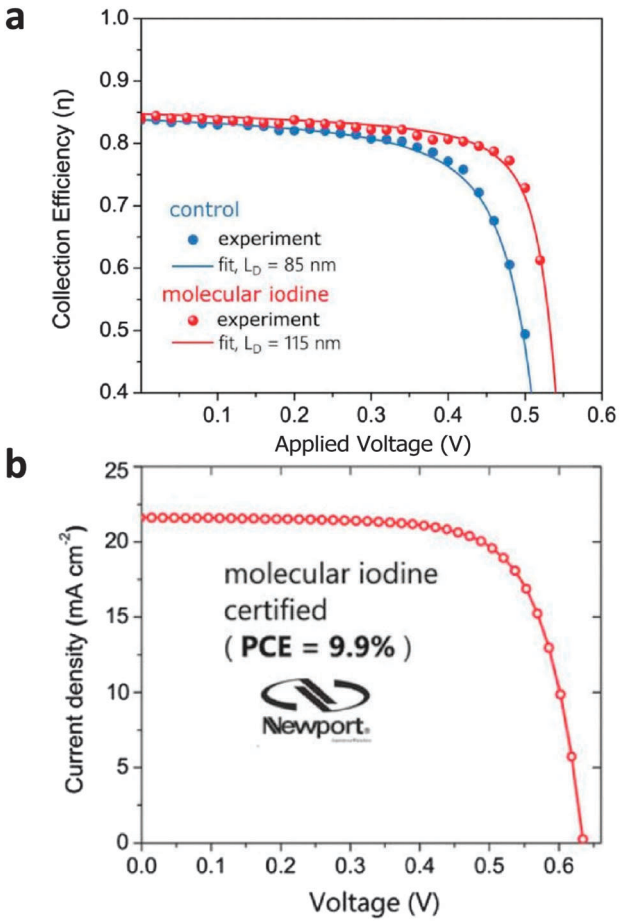

Fig. 11 (a) Collection efficiency and diffusion length for control and molecular I_2-treated CQDs. A 35% increase is observed for I_2 treated devices. (b) Measured current–voltage characteristics under certified AM1.5 simulated solar illumination. Reprinted with permission from ref. 105. Copyright 2015 John Wiley and Sons.

solid-state organic ligand exchange. Halide anions are introduced *in situ* or during the end stages of the synthesis process, allowing the passivation of sites inaccessible to bulkier organic ligands. Small organic ligands such as MPA and EDT are then used in the solid state to replace long organic ligands.

The hybrid passivation step (photoluminescence spectra in Fig. 13a) leads to preservation of the fluorescence peak positions in both solution and films. Decreased trap-associated long-wavelength photoluminescence was observed for the hybrid case compared to the organic one. The midgap trap state density inside the hybrid passivated film was 2×10^{16} cm^{-3} eV^{-1}, one order of magnitude lower than those from either organic ligands or inorganic ligands used alone (Fig. 13b). The film carrier mobility was increased as the defect density was reduced. As a consequence, both the voltage and current of the device were enhanced, leading to a 1.2× increase in PCE.

For in-synthesis hybrid passivation, metal halides were used as a precursor for CQD growth. The device performance improvement based on this technique was similar to that using the post-synthesis treatment.[53] Recently, combining the cation exchange synthesis and the hybrid ligand strategy led to a PCE

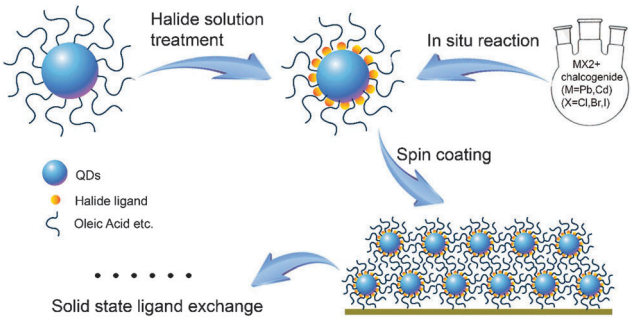

Fig. 12 Schematic diagram of the two kinds of method for hybrid ligand passivation and film fabrication process. For the first method, the halide treatment was made after CQD synthesis. In the second method, the halide treatment was made right after the CQDs growth in synthesis. After halide treatment in solution state, film deposition was carried out by spin coating, followed with solid-state ligand exchange.

greater than 7% in 2012, a notable record at that time.[108] The combination of the solution-phase halide and the short thiol crosslinker treatment produces a 1.15× increase of PCE over relevant controls.[111] Overall, as a result of its significant reduction of surface defects, the hybrid passivating strategy yields higher voltage and PCE compared with all-organic strategies.

The role of the organic ligands remained important, with crosslinkers such as MPA bringing denser films following solid-state treatments. The interdot distance in film is measured using grazing-incidence small-angle X-ray spectroscopy (GISAXS) (Fig. 13c and d).[108] The distances following MPA treatments were appreciably shorter than when halide ligands alone were used; and also compared to EDT crosslinking. The close packing was important for higher carrier mobility, a contributor to increased PCE using MPA ligands.[70]

The hybrid passivation strategy was explored for CQD sensitized solar cells as well, also with the goal of reducing surface defects. For CdSe CQD sensitized solar cells, the efficiency was improved by about 1.4× *via* the addition of halides to MPA-ligated CQDs.[112] For PbS/CdS/ZnS sensitized solar cells, the use of both EDT and iodide ligands together brought efficiency to 4.7%, about 10% higher than control devices made using a single type of ligand.[78]

5. Colloidal quantum dots in perovskite

Compared with organic ligands, MCC ligands effectively improve film conductivity, while halide ligands reduce defect density. However, ligand loss in exchange process is still one major issue that limits device performance.

A strategy was recently devised to overcome these limitations: a complete *in situ* ligand application in solution, followed by growth of a heteroepitaxial ligand/matrix from the solution-applied ligand/matrix precursors as part of the final film-forming process. Using a heteroepitaxial matrix offers a path to excellent surface passivation combined with excellent carrier transport, a combination achievable when the matrix materials produce a matched lattice type and constant relative to the CQD surfaces (Fig. 14).

The organic–inorganic hybrid perovskite $CH_3NH_3PbI_3$ has the same cubic crystal structure and a very similar lattice constant

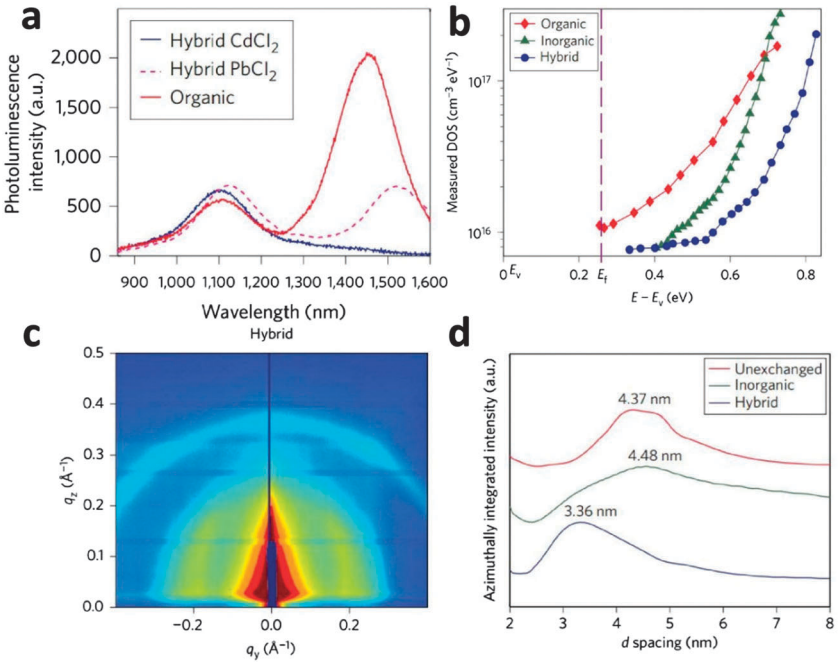

Fig. 13 (a) Photoluminescence of CQD film with organic (red), $PbCl_2$ hybrid (pink) and $CdCl_2$ hybrid (blue) passivation. A marked decrease in trap-associated long wavelength photoluminescence is observed from the organic to the hybrid case. (b) Density of state (DOS) in the bandgap calculated from transient photovoltage measurements for organic (red), inorganic (green) and hybrid (blue) passivation of PbS CQD films. (c) GISAXS pattern of the film with hybrid passivation. (d) The average interparticle spacing for unexchanged CQD film, CQD film with inorganic ligand and CQD film with hybrid ligand. With hybrid ligand, the distance is much shorter than the other two. Reprinted with permission from ref. 108. Copyright the Nature Publishing Group 2012.

as PbS, and was for this reason explored as a candidate matrix. The film fabrication procedure is shown in Fig. 15a. PbI_2 salts were mixed with the CQD ink. Film were spin-cast, after which they were treated using CH_3NH_3I solution to enable the growth of perovskite matrix *via* reaction with the incorporated PbI_2 matrix/ligand combination. The absorption and the emission spectra of CQDs were maintained following perovskite growth (Fig. 15b). The diffusion length of the CQD/perovskite hybrid materials decreased with the increase of CQD concentration, indicating efficient carrier transfer from perovskite into CQDs.

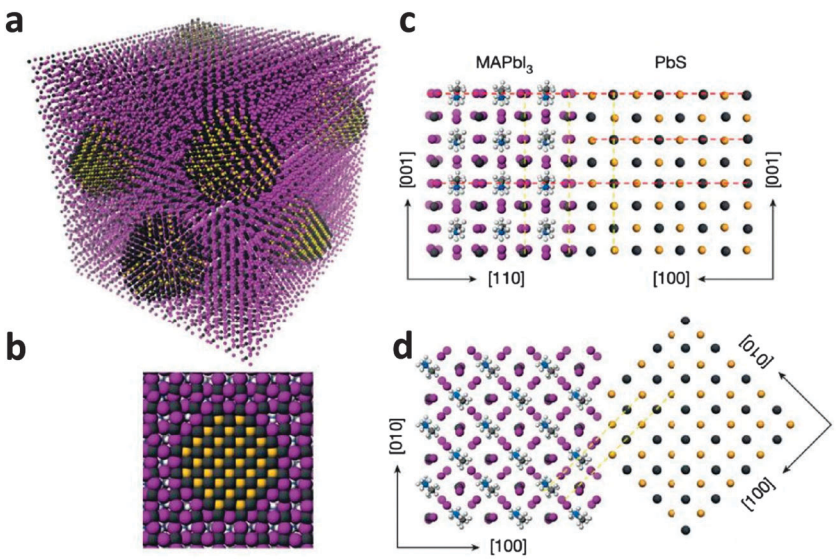

Fig. 14 (a) 3D atomistic model of CQDs in a perovskite matrix. (b) 2D view of a single CQD in perovskite. Modelling of PbS and MAPbI3 crystal structure and their interface, showing that perovskite matches well with PbS in both the X–Z plane (c) and the X–Y plane (d). The red dashes show the unit cell size; the yellow dashes are guides to the eye for matching planes. (colours represent the following: grey, lead; purple, iodine; yellow, sulfur.) Reprinted with permission from ref. 48. Copyright the Nature Publishing Group 2015.

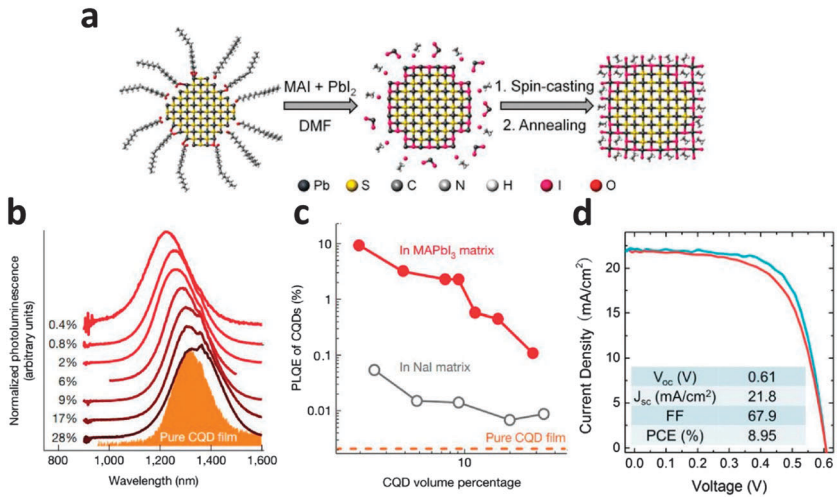

Fig. 15 (a) Schematic diagram of ligand exchange and film fabrication process. (b) Photoluminescence of the CQD–perovskite hybrid. The different curves correspond to different CQD volume percentages, CQD photoluminescence exciton peaks is preserved, indicating that the properties of CQDs remain unaltered. (c) Photoluminescence quantum efficiency (PLQE) of CQDs in matrix. In the $MAPbI_3$ matrix, the PLQE is two orders of magnitude higher than that in a NaI matrix, and 3000 times greater than in pure CQD film with iodide ligands. (d) Measured current–voltage curves under AM1.5 simulated solar illumination for representative devices. 8.95% PCE was achieved for CQD ink for the first time. (a and d) Was reprinted with permission from ref. 113. Copyright 2015 American Chemical Society. (b and c) Was reprinted with permission from ref. 48. Copyright 2015 Nature Publishing Group.

The epitaxial growth of perovskite on the CQD surface was confirmed using selective area electron diffraction (SAED) measurements; and by the observation of a 100× improvement in the film PLQY compared to a pure CQD film, and also compared to a dot-in-matrix film employing a nonepitaxial (NaI) matrix (Fig. 15c). The high carrier mobility of the perovskite matrix enabled efficient carrier transport; and, *via* energy level engineering, carriers were injected from the perovskite matrix into CQDs embedded therein. This strategy is relevant to both LEDs and lasers, and is of particular interest in the infrared regime 800–1500 nm in which optical sources are needed and present-day solution-processed device performance is relatively low.[48]

The perovskite liganding strategy was also extended to a thin-shell approach to passivate CQD surfaces for solar cell application. Here the defect density was reduced and the carrier diffusion length increased relative to controls. The overall PCE was improved to almost 9%,[113] the current record for CQD-ink-based solar cells (Fig. 15d).

In situ epitaxial growth provided therefore a new strategy to passivate CQD surfaces inside films, overcoming the prior problem of ligand loss in the course of the film fabrication process. It provides new avenues to the development of high-performance CQD-based optoelectronic sources relevant to actively-illuminated night vision, biomedical imaging, and fiber-optic communications.

Conclusion

This review summarized recent developments in CQD surface engineering relevant to solar photovoltaics. The performance of CQD-based solar cells has improved principally *via* systematic surface engineering studies. The use of halide ligands during solid-state CQD ligand exchange improves carrier mobility and also decreases recombination centers. It also enables tuning of electronic properties, enabling device developments such as graded doping. The advent of perovskite matrices for CQDs provides an exciting new degree of freedom in CQD surfaces management in solids. MCC ligands are responsible for recent records in FET carrier mobilities. The use of core/shell structures and longer thiol ligands has drive the latest progress in EL devices based on CQDs. The perovskite matrix is relevant here too, for it provides a means to maximize PLQY without sacrificing carrier mobility.

With recombination center densities now approaching 10^{15} cm^{-3} (1 per $(100\ nm)^3$ cube, corresponding to ~one per $\sim 10^4$ quantum dots), the field may now be approaching the regime in which further advances in minority carrier diffusion length require improvements to qualities other than the nanoparticle surface. A roadmap for device performance (Fig. 16) suggests entry into a regime in which carrier mobility merits renewed focus. One important frontier will be the examination of the bulk crystal making up each CQD, in which vacancies, interstitials, and rare impurities introduced in synthesis merit renewed attention. In parallel, since size dispersity produces bandgap-dispersity in the CQD ensemble, a renewed focus on monodispersity, and the maintenance of size, shape, and coupling strength consistency across the quantum dot solid, deserve new focus. At a device level, increasing the effective path length of a typical solar photon through the CQD solid, beyond the double-pass seen in unenhanced round-trip reflection from the back contact, represents an undertapped and highly rewarding territory. Additionally, delicate band alignment engineering between electron acceptor layer and CQD active layer gives another possibility to improve device performance.

The realization of commercial application of CQD solar cells requires a number of materials processing, scale-up, and stability

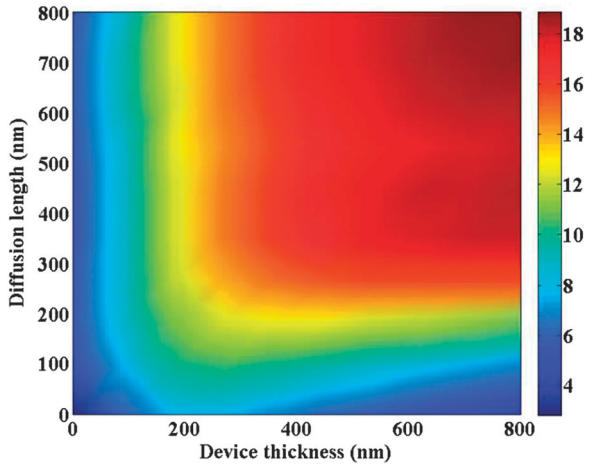

Fig. 16 Theoretic prediction of solar cells performance. With the increase of diffusion length, the efficiency of solar cells can be significantly improved, indicating a pathway to get efficiency close to 20%.

challenges to be addressed. Inkjet printing[114,115] and spray coating[116] have recently been explored in the deposition of CQDs over large areas, and these have been shown to bring similar performance to that obtained using R&D-lab-scale spin-coating. These suggest avenues to roll-to-roll processing that can be automated setups for reproducible deposition of CQD films over large areas. The stability of devices under extended illumination demands further investigation, though improved stability has been achieved based on the ligand engineering discussed above, such as encouraging stability in air for over 150 days. The cost CQD solar cells at scaled-up manufacture is an important factor in their adoption, and is challenging to estimate with precision in light of its dependence on volume (as opposed to small-scale) materials costs; and given the role of labor and capital costs. Coarse extrapolations based on present-day materials costs, and assuming a high degree of automation (*e.g.* flow-reactor) in synthesis,[117] suggests avenues to CQD films at $< \$10$ per m^{-2} of solar cell area.

Acknowledgements

Z. N acknowledges start-up funding from ShanghaiTech University, The Young 1000 Talents Program, and NSFC (21571129). E. H. S acknowledges support from award KUS-11-009-21 from King Abdullah University of Science and Technology (KAUST), from the Ontario Research Fund – Research Excellence Program, from the Natural Sciences and Engineering Research Council (NSERC) of Canada, and from the International Cooperation of the Korea Institute of Energy Technology Evaluation and Planning (KETEP) grant funded by the Korea government Ministry of Knowledge Economy (2012T100100740). P. K. acknowledges support from Faculty of Science, Mahidol University, the Thailand Research Fund (TRF), and the National Nanotechnology Center (NANOTEC), NSTDA, Ministry of Science and Technology, Thailand, through its program of Centers of Excellence Network. We thank Dr. Oleksandr Voznyy for helpful discussion about device performance simulation.

References

1 C. Murray, D. J. Norris and M. G. Bawendi, *J. Am. Chem. Soc.*, 1993, **115**, 8706–8715.
2 M. A. Hines and G. D. Scholes, *Adv. Mater.*, 2003, **15**, 1844–1849.
3 L. Li, A. Pandey, D. J. Werder, B. P. Khanal, J. M. Pietryga and V. I. Klimov, *J. Am. Chem. Soc.*, 2011, **133**, 1176–1179.
4 J. A. Scholl, A. L. Koh and J. A. Dionne, *Nature*, 2012, **483**, 421–427.
5 A. J. Nozik, *Physica E*, 2002, **14**, 115–120.
6 A. J. Nozik, *Chem. Phys. Lett.*, 2008, **457**, 3–11.
7 R. D. Schaller and V. I. Klimov, *Phys. Rev. Lett.*, 2004, **92**, 186601.
8 A. J. Nozik, M. C. Beard, J. M. Luther, M. Law, R. J. Ellingson and J. C. Johnson, *Chem. Rev.*, 2010, **110**, 6873–6890.
9 H. W. Hillhouse and M. C. Beard, *Curr. Opin. Colloid Interface Sci.*, 2009, **14**, 245–259.
10 B. Ehrler, M. W. B. Wilson, A. Rao, R. H. Friend and N. C. Greenham, *Nano Lett.*, 2012, **12**, 1053–1057.
11 Z. Ning, H. Tian, H. Qin, Q. Zhang, H. Ågren, L. Sun and Y. Fu, *J. Phys. Chem. C*, 2010, **114**, 15184–15189.
12 V. Sukhovatkin, S. Hinds, L. Brzozowski and E. H. Sargent, *Science*, 2009, **324**, 1542–1544.
13 S. A. Mcdonald, G. Konstantatos, S. Zhang, P. W. Cyr, E. J. Klem, L. Levina and E. H. Sargent, *Nat. Mater.*, 2005, **4**, 138–142.
14 Y. Yang, Y. Zheng, W. Cao, A. Titov, J. Hyvonen, R. MandersJesse, J. Xue, P. H. Holloway and L. Qian, *Nat. Photonics*, 2015, **9**, 259–266.
15 F. Zhang, H. Zhong, C. Chen, X.-g. Wu, X. Hu, H. Huang, J. Han, B. Zou and Y. Dong, *ACS Nano*, 2015, **9**, 4533–4542.
16 V. Wood, M. J. Panzer, J. Chen, M. S. Bradley, J. E. Halpert, M. G. Bawendi and V. Bulovic, *Adv. Mater.*, 2009, **21**, 2151–2155.
17 G. H. Kim, F. P. Garcia de Arquer, Y. J. Yoon, X. Lan, M. Liu, O. Voznyy, Z. Yang, F. Fan, A. H. Ip, P. Kanjanaboos, S. Hoogland, J. Y. Kim and E. H. Sargent, *Nano Lett.*, 2015, **15**, 7691–7696.
18 M. L. Böhm, T. C. Jellicoe, M. Tabachnyk, N. J. L. K. Davis, F. Wisnivesky-Rocca-Rivarola, C. Ducati, B. Ehrler, A. A. Bakulin and N. C. Greenham, *Nano Lett.*, 2015, **15**, 7987–7993.
19 http://www.qdvision.com/products.
20 X. Dai, Z. Zhang, Y. Jin, Y. Niu, H. Cao, X. Liang, L. Chen, J. Wang and X. Peng, *Nature*, 2014, **515**, 96–99.
21 N.-M. Park, T.-S. Kim and S.-J. Park, *Appl. Phys. Lett.*, 2001, **78**, 2575–2577.
22 Q. Sun, Y. A. Wang, L. S. Li, D. Wang, T. Zhu, J. Xu, C. Yang and Y. Li, *Nat. Photonics*, 2007, **1**, 717–722.
23 Y. Shirasaki, G. J. Supran, M. G. Bawendi and V. Bulović, *Nat. Photonics*, 2013, **7**, 13–23.
24 J. Jang, D. S. Dolzhnikov, W. Liu, S. Nam, M. Shim and D. V. Talapin, *Nano Lett.*, 2015, **15**, 6309–6317.
25 https://invisage.us/.
26 J. Zhang, J. Gao, C. P. Church, E. M. Miller, J. M. Luther, V. I. Klimov and M. C. Beard, *Nano Lett.*, 2014, **14**, 6010–6015.
27 A. G. Pattantyus-Abraham, I. J. Kramer, A. R. Barkhouse, X. Wang, G. Konstantatos, R. Debnath, L. Levina, I. Raabe, M. K. Nazeeruddin and M. Gratzel, *ACS Nano*, 2010, **4**, 3374–3380.
28 J. Shi, P. Zhao and X. Wang, *Adv. Mater.*, 2013, **25**, 916–921.

29 P. V. Kamat, K. Tvrdy, D. R. Baker and J. G. Radich, *Chem. Rev.*, 2010, **110**, 6664–6688.
30 G. Chen, J. Seo, C. Yang and P. N. Prasad, *Chem. Soc. Rev.*, 2013, **42**, 8304–8338.
31 O. E. Semonin, J. M. Luther and M. C. Beard, *Mater. Today*, 2012, **15**, 508–515.
32 B. Ehrler, M. W. Wilson, A. Rao, R. H. Friend and N. C. Greenham, *Nano Lett.*, 2012, **12**, 1053–1057.
33 H. Zhang, J. S. Son, J. Jang, J.-S. Lee, W.-L. Ong, J. A. Malen and D. V. Talapin, *ACS Nano*, 2013, **7**, 10296–10306.
34 J. S. Son, H. Zhang, J. Jang, B. Poudel, A. Waring, L. Nally and D. V. Talapin, *Angew. Chem., Int. Ed.*, 2014, **53**, 7466–7470.
35 M. Ibanez, R. J. Korkosz, Z. Luo, P. Riba, D. Cadavid, S. Ortega, A. Cabot and M. G. Kanatzidis, *J. Am. Chem. Soc.*, 2015, **137**, 4046–4049.
36 M. Ibáñez, R. Zamani, S. Gorsse, J. Fan, S. Ortega, D. Cadavid, J. R. Morante, J. Arbiol and A. Cabot, *ACS Nano*, 2013, **7**, 2573–2586.
37 R. Y. Wang, J. P. Feser, J.-S. Lee, D. V. Talapin, R. Segalman and A. Majumdar, *Nano Lett.*, 2008, **8**, 2283–2288.
38 I. Moreels, K. Lambert, D. Smeets, D. De Muynck, T. Nollet, J. C. Martins, F. Vanhaecke, A. Vantomme, C. Delerue, G. Allan and Z. Hens, *ACS Nano*, 2009, **3**, 3023–3030.
39 N. N. Ledentsov, *Semicond. Sci. Technol.*, 2011, **26**, 014001.
40 S. Hoogland, V. Sukhovatkin, I. Howard, S. Cauchi, L. Levina and E. H. Sargent, *Opt. Express*, 2006, **14**, 3273–3281.
41 M. C. Schlamp, X. Peng and A. P. Alivisatos, *J. Appl. Phys.*, 1997, **82**, 5837–5842.
42 D. L. Klein, R. Roth, A. K. L. Lim, A. P. Alivisatos and P. L. McEuen, *Nature*, 1997, **389**, 699–701.
43 W. U. Huynh, X. Peng and A. P. Alivisatos, *Adv. Mater.*, 1999, **11**, 923–927.
44 G. Konstantatos, I. Howard, A. Fischer, S. Hoogland, J. Clifford, E. Klem, L. Levina and E. H. Sargent, *Nature*, 2006, **442**, 180–183.
45 L. Huang, C.-C. Tu and L. Y. Lin, *Appl. Phys. Lett.*, 2011, **98**, 113110.
46 D. V. Talapin and C. B. Murray, *Science*, 2005, **310**, 86–89.
47 G. H. Carey, A. L. Abdelhady, Z. Ning, S. M. Thon, O. M. Bakr and E. H. Sargent, *Chem. Rev.*, 2015, **115**, 12732–12763.
48 Z. Ning, X. Gong, R. Comin, G. Walters, F. Fan, O. Voznyy, E. Yassitepe, A. Buin, S. Hoogland and E. H. Sargent, *Nature*, 2015, **523**, 324–328.
49 D. Yanover, R. K. Čapek, A. Rubin-Brusilovski, R. Vaxenburg, N. Grumbach, G. I. Maikov, O. Solomeshch, A. Sashchiuk and E. Lifshitz, *Chem. Mater.*, 2012, **24**, 4417–4423.
50 D. V. Talapin, I. Mekis, S. Götzinger, A. Kornowski, O. Benson and H. Weller, *J. Phys. Chem. B*, 2004, **108**, 18826–18831.
51 L. Li, A. Pandey, D. J. Werder, B. P. Khanal, J. M. Pietryga and V. I. Klimov, *J. Am. Chem. Soc.*, 2011, **133**, 1176–1179.
52 J. Zhang, R. W. Crisp, J. Gao, D. M. Kroupa, M. C. Beard and J. M. Luther, *J. Phys. Chem. Lett.*, 2015, **6**, 1830–1833.
53 J. Zhang, J. Gao, E. M. Miller, J. M. Luther and M. C. Beard, *ACS Nano*, 2014, **8**, 614–622.
54 V. Sayevich, N. Gaponik, M. Plötner, M. Kruszynska, T. Gemming, V. M. Dzhagan, S. Akhavan, D. R. T. Zahn, H. V. Demir and A. Eychmüller, *Chem. Mater.*, 2015, **27**, 4328–4337.
55 A. Stavrinadis, A. K. Rath, F. P. de Arquer, S. L. Diedenhofen, C. Magen, L. Martinez, D. So and G. Konstantatos, *Nat. Commun.*, 2013, **4**, 2981.
56 P. R. Brown, R. R. Lunt, N. Zhao, T. P. Osedach, D. D. Wanger, L. Y. Chang, M. G. Bawendi and V. Bulovic, *Nano Lett.*, 2011, **11**, 2955–2961.
57 K. S. Jeong, J. Tang, H. Liu, J. Kim, A. W. Schaefer, K. Kemp, L. Levina, X. Wang, S. Hoogland and R. Debnath, *ACS Nano*, 2011, **6**, 89–99.
58 R. W. Crisp, D. M. Kroupa, A. R. Marshall, E. M. Miller, J. Zhang, M. C. Beard and J. M. Luther, *Sci. Rep.*, 2015, **5**, 9945.
59 J. M. Luther, M. Law, Q. Song, C. L. Perkins, M. C. Beard and A. J. Nozik, *ACS Nano*, 2008, **2**, 271–280.
60 G. I. Koleilat, L. Levina, H. Shukla, S. H. Myrskog, S. Hinds, A. G. Pattantyus-Abraham and E. H. Sargent, *ACS Nano*, 2008, **2**, 833–840.
61 L. Y. Chang, R. R. Lunt, P. R. Brown, V. Bulovic and M. G. Bawendi, *Nano Lett.*, 2013, **13**, 994–999.
62 J. P. Clifford, K. W. Johnston, L. Levina and E. H. Sargent, *Appl. Phys. Lett.*, 2007, **91**, 253117.
63 M.-Q. Dai and L.-Y. L. Yung, *Chem. Mater.*, 2013, **25**, 2193–2201.
64 J. M. Luther, M. Law, Q. Song, C. L. Perkins, M. C. Beard and A. J. Nozik, *ACS Nano*, 2008, **2**, 271–280.
65 J. J. Choi, W. N. Wenger, R. S. Hoffman, Y. F. Lim, J. Luria, J. Jasieniak, J. A. Marohn and T. Hanrath, *Adv. Mater.*, 2011, **23**, 3144–3148.
66 R. Debnath, J. Tang, D. A. Barkhouse, X. Wang, A. G. Pattantyus-Abraham, L. Brzozowski, L. Levina and E. H. Sargent, *J. Am. Chem. Soc.*, 2010, **132**, 5952–5953.
67 K. W. Johnston, A. G. Pattantyus-Abraham, J. P. Clifford, S. H. Myrskog, D. D. MacNeil, L. Levina and E. H. Sargent, *Appl. Phys. Lett.*, 2008, **92**, 151115.
68 H. Liu, J. Tang, I. J. Kramer, R. Debnath, G. I. Koleilat, X. Wang, A. Fisher, R. Li, L. Brzozowski, L. Levina and E. H. Sargent, *Adv. Mater.*, 2011, **23**, 3832–3837.
69 D. A. Barkhouse, R. Debnath, I. J. Kramer, D. Zhitomirsky, A. G. Pattantyus-Abraham, L. Levina, L. Etgar, M. Gratzel and E. H. Sargent, *Adv. Mater.*, 2011, **23**, 3134–3138.
70 K. S. Jeong, J. Tang, H. Liu, J. Kim, A. W. Schaefer, K. Kemp, L. Levina, X. Wang, S. Hoogland, R. Debnath, L. Brzozowski, E. H. Sargent and J. B. Asbury, *ACS Nano*, 2012, **6**, 89–99.
71 C. Giansante, L. Carbone, C. Giannini, D. Altamura, Z. Ameer, G. Maruccio, A. Loiudice, M. R. Belviso, P. D. Cozzoli, A. Rizzo and G. Gigli, *J. Phys. Chem. C*, 2013, **117**, 13305–13317.
72 Z. Ning, O. Voznyy, J. Pan, S. Hoogland, V. Adinolfi, J. Xu, M. Li, A. R. Kirmani, J.-P. Sun, J. Minor, K. W. Kemp, H. Dong, L. Rollny, A. Labelle, G. Carey, B. Sutherland, I. Hill, A. Amassian, H. Liu, J. Tang, O. M. Bakr and E. H. Sargent, *Nat. Mater.*, 2014, **13**, 822–828.
73 A. Fischer, L. Rollny, J. Pan, G. H. Carey, S. M. Thon, S. Hoogland, O. Voznyy, D. Zhitomirsky, J. Y. Kim and O. M. Bakr, *Adv. Mater.*, 2013, **25**, 5742–5749.
74 J. Y. Kim, V. Adinolfi, B. R. Sutherland, O. Voznyy, S. J. Kwon, T. W. Kim, J. Kim, H. Ihee, K. Kemp, M. Adachi, M. Yuan, I. Kramer, D. Zhitomirsky, S. Hoogland and E. H. Sargent, *Nat. Commun.*, 2015, **6**, 7772.

75 I. Robel, V. Subramanian, M. Kuno and P. V. Kamat, *J. Am. Chem. Soc.*, 2006, **128**, 2385–2393.
76 J. Wang, I. Mora-Seró, Z. Pan, K. Zhao, H. Zhang, Y. Feng, G. Yang, X. Zhong and J. Bisquert, *J. Am. Chem. Soc.*, 2013, **135**, 15913–15922.
77 J. Huang, B. Xu, C. Yuan, H. Chen, J. Sun, L. Sun and H. Ågren, *ACS Appl. Mater. Interfaces*, 2014, **6**, 18808–18815.
78 M. S. de la Fuente, R. S. Sanchez, V. Gonzalez-Pedro, P. P. Boix, S. G. Mhaisalkar, M. E. Rincon, J. Bisquert and I. Mora-Sero, *J. Phys. Chem. Lett.*, 2013, **4**, 1519–1525.
79 A. N. Jumabekov, N. Cordes, T. D. Siegler, P. Docampo, A. Ivanova, K. Fominykh, D. D. Medina, L. M. Peter and T. Bein, *ACS Appl. Mater. Interfaces*, 2016, **8**, 4600–4607.
80 X. Yang, K. Dev, J. Wang, E. Mutlugun, C. Dang, Y. Zhao, S. Liu, Y. Tang, S. T. Tan and X. W. Sun, *Adv. Funct. Mater.*, 2014, **24**, 5977–5984.
81 J. Kwak, J. Lim, M. Park, S. Lee, K. Char and C. Lee, *Nano Lett.*, 2015, **15**, 3793–3799.
82 J. Lim, B. G. Jeong, M. Park, J. K. Kim, J. M. Pietryga, Y. S. Park, V. I. Klimov, C. Lee, D. C. Lee and W. K. Bae, *Adv. Mater.*, 2014, **26**, 8034–8040.
83 L. Sun, J. J. Choi, D. Stachnik, A. C. Bartnik, B.-R. Hyun, G. G. Malliaras, T. Hanrath and F. W. Wise, *Nat. Nanotechnol.*, 2012, **7**, 369–373.
84 M. V. Kovalenko, M. Scheele and D. V. Talapin, *Science*, 2009, **324**, 1417–1420.
85 A. Nag, H. Zhang, E. Janke and D. V. Talapin, *Z. Phys. Chem.*, 2015, **229**, 85–107.
86 J. Li, H. Shen, C. Zhou, N. Li, H. Wang and L. S. Li, *J. Nanopart. Res.*, 2014, **16**, 2802.
87 W. Liu, J. S. Lee and D. V. Talapin, *J. Am. Chem. Soc.*, 2013, **135**, 1349–1357.
88 M. V. Kovalenko, M. I. Bodnarchuk, J. Zaumseil, J.-S. Lee and D. V. Talapin, *J. Am. Chem. Soc.*, 2010, **132**, 10085–10092.
89 M. V. Kovalenko, R. D. Schaller, D. Jarzab, M. A. Loi and D. V. Talapin, *J. Am. Chem. Soc.*, 2012, **134**, 2457–2460.
90 C. Jiang, J. S. Lee and D. V. Talapin, *J. Am. Chem. Soc.*, 2012, **134**, 5010–5013.
91 A. Nag, M. V. Kovalenko, J. S. Lee, W. Liu, B. Spokoyny and D. V. Talapin, *J. Am. Chem. Soc.*, 2011, **133**, 10612–10620.
92 J. Huang, W. Liu, D. S. Dolzhnikov, L. Protesescu, M. V. Kovalenko, B. Koo, S. Chattopadhyay, E. V. Shenchenko and D. V. Talapin, *ACS Nano*, 2014, **8**, 9388–9402.
93 J.-S. Lee, M. V. Kovalenko, J. Huang, D. S. Chung and D. V. Talapin, *Nat. Nanotechnol.*, 2011, **6**, 348–352.
94 D. S. Dolzhnikov, H. Zhang, J. Jang, J. S. Son, M. G. Panthani, T. Shibata, S. Chattopadhyay and D. V. Talapin, *Science*, 2015, **347**, 425–428.
95 J. Tang, K. W. Kemp, S. Hoogland, K. S. Jeong, H. Liu, L. Levina, M. Furukawa, X. Wang, R. Debnath, D. Cha, K. W. Chou, A. Fischer, A. Amassian, J. B. Asbury and E. H. Sargent, *Nat. Mater.*, 2011, **10**, 765–771.
96 R. G. Pearson, *J. Am. Chem. Soc.*, 1963, **85**, 3533–3539.
97 Y. Zhang, D. Zherebetskyy, N. D. Bronstein, S. Barja, L. Lichtenstein, A. P. Alivisatos, L.-W. Wang and M. Salmeron, *ACS Nano*, 2015, **9**, 10445–10452.
98 D. Zherebetskyy, M. Scheele, Y. Zhang, N. Bronstein, C. Thompson, D. Britt, M. Salmeron, P. Alivisatos and L.-W. Wang, *Science*, 2014, **344**, 1380–1384.
99 O. Voznyy, D. Zhitomirsky, P. Stadler, Z. Ning, S. Hoogland and E. H. Sargent, *ACS Nano*, 2012, **6**, 8448–8455.
100 Z. Ning, D. Zhitomirsky, V. Adinolfi, B. Sutherland, J. Xu, O. Voznyy, P. Maraghechi, X. Lan, S. Hoogland, Y. Ren and E. H. Sargent, *Adv. Mater.*, 2013, **25**, 1719–1723.
101 C. H. Chuang, P. R. Brown, V. Bulovic and M. G. Bawendi, *Nat. Mater.*, 2014, **13**, 796–801.
102 D. J. Milliron, *Nat. Mater.*, 2014, **13**, 772–773.
103 Z. Ning, Y. Ren, S. Hoogland, O. Voznyy, L. Levina, P. Stadler, X. Lan, D. Zhitomirsky and E. H. Sargent, *Adv. Mater.*, 2012, **24**, 6295–6299.
104 X. Lan, O. Voznyy, A. Kiani, F. P. García de Arquer, A. S. Abbas, G. H. Kim, M. Liu, Z. Yang, G. Walters and J. Xu, *Adv. Mater.*, 2015, 1–7.
105 P. Wei, T. Menke, B. D. Naab, K. Leo, M. Riede and Z. Bao, *J. Am. Chem. Soc.*, 2012, **134**, 3999–4002.
106 G. Niu, L. Wang, R. Gao, W. Li, X. Guo, H. Dong and Y. Qiu, *Phys. Chem. Chem. Phys.*, 2013, **15**, 19595–19600.
107 D. N. Dirin, S. Dreyfuss, M. I. Bodnarchuk, G. Nedelcu, P. Papagiorgis, G. Itskos and M. V. Kovalenko, *J. Am. Chem. Soc.*, 2014, **136**, 6550–6553.
108 A. H. Ip, S. M. Thon, S. Hoogland, O. Voznyy, D. Zhitomirsky, R. Debnath, L. Levina, L. R. Rollny, G. H. Carey, A. Fischer, K. W. Kemp, I. J. Kramer, Z. Ning, A. J. Labelle, K. W. Chou, A. Amassian and E. H. Sargent, *Nat. Nanotechnol.*, 2012, **7**, 577–582.
109 S. Kim, A. R. Marshall, D. M. Kroupa, E. M. Miller, J. M. Luther, S. Jeong and M. C. Beard, *ACS Nano*, 2015, **9**, 8157–8164.
110 M. L. Böhm, T. C. Jellicoe, J. P. H. Rivett, A. Sadhanala, N. J. L. K. Davis, F. S. F. Morgenstern, K. C. Gödel, J. Govindasamy, C. G. M. Benson, N. C. Greenham and B. Ehrler, *J. Phys. Chem. Lett.*, 2015, **6**, 3510–3514.
111 D. Zhitomirsky, O. Voznyy, L. Levina, S. Hoogland, K. W. Kemp, A. H. Ip, S. M. Thon and E. H. Sargent, *Nat. Commun.*, 2014, **5**, 3803.
112 J. Huang, B. Xu, C. Yuan, H. Chen, J. Sun, L. Sun and H. Agren, *ACS Appl. Mater. Interfaces*, 2014, **6**, 18808–18815.
113 Z. Yang, A. Janmohamed, X. Lan, F. P. García de Arquer, O. Voznyy, E. Yassitepe, G.-H. Kim, Z. Ning, X. Gong, R. Comin and E. H. Sargent, *Nano Lett.*, 2015, **15**, 7539–7543.
114 V. Wood, M. J. Panzer, J. Chen, M. S. Bradley, J. E. Halpert, M. G. Bawendi and V. Bulović, *Adv. Mater.*, 2009, **21**, 2151–2155.
115 Q. Guo, S. J. Kim, M. Kar, W. N. Shafarman, R. W. Birkmire, E. A. Stach, R. Agrawal and H. W. Hillhouse, *Nano Lett.*, 2008, **8**, 2982–2987.
116 I. J. Kramer, J. C. Minor, G. Moreno-Bautista, L. Rollny, P. Kanjanaboos, D. Kopilovic, S. M. Thon, G. H. Carey, K. W. Chou and D. Zhitomirsky, *Adv. Mater.*, 2015, **27**, 116–121.
117 A. Fischer, L. Rollny, J. Pan, G. H. Carey, S. M. Thon, S. Hoogland, O. Voznyy, D. Zhitomirsky, J. Y. Kim, O. M. Bakr and E. H. Sargent, *Adv. Mater.*, 2013, **25**, 5742–5749.

